Generalized viscosity, pair potential, and memory functions from $S(q,\omega)$ measurements for liquid metals

Karl-Erik Larsson and Waclaw Gudowski
Royal Institute of Technology, S-100 44 Stockholm, Sweden
(Received 19 September 1985)

The aim of the present work is to perform an in-depth analysis of neutron scattering data on liquid metals and to extend previous types of comparisons between experimental scattering functions and various model theories. The kinematic viscosity $\nu(q)$ for some liquid metals—liquid lead at 623 and 1173 K, liquid bismuth at 578 K, and liquid rubidium at 315 K—is derived, based on the dynamical scattering functions $S(q,\omega)$, and compared to molecular dynamics data for hard spheres. The general behavior of the $\nu(q)$ curve is traced. With use of an analytical form of pair potential with several free parameters, a form of $V(r)$ for liquid lead at 623 K is derived. Finally, the short-time interaction part of the experimental memory function $\Phi_l(q,t)$ for the longitudinal current correlation function is directly compared to the corresponding result calculated from kinetic theory in the mode-coupling version. This comparison is based upon the derived form of the interatomic potential for Pb at 623 K and upon other known potential data for Rb at 315 K.

I. INTRODUCTION

In recent years intense discussion has existed regarding the theoretical description of atomic motions in liquids. The generalization of linear hydrodynamics to make this mathematical framework usable down to atomic distances has been advocated based mainly on results from molecular dynamics[1-3] (MD) using continuous potentials as well as from hard-sphere systems. The hydrodynamic equations are recast into Mori's memory-function formalism to establish close contact with the ideas of viscoelastic behavior. Deeper insight and more detailed information about both the short-time viscoelastic behavior dominated by the binary collision and various types of backflow of hydrodynamic nature set up around a moving atom are obtained from kinetic theory in its mode-coupling versions.[4,5] The only *direct* experimental check was with the scattering function $S(q,\omega)$ obtained from the neutron scattering experiments. $S(q,\omega)$ was calculated theoretically, and this result was compared to the neutron result, but more often, MD results based upon assumed pair potentials served as a basis for comparison.

For a long period of time the interest in neutron measurements concentrated on smaller wave-vector regions such that zero sound or so-called Brillouin side peaks could be observed in $S(q,\omega)$—in the region $q/q_0 < \frac{2}{3}$, where q_0 is the value of q at the peak of the structure factor, $S(q)$.[6] This region in the (q,ω) plane is very difficult to explore because $S(q,\omega)$ reaches only very small values. Comparisons between theories and experiments were also made in the main region of $S(q,\omega)$ for $0.8 < q/q_0 < 3.5$, within which more accurate neutron scattering experiments for determination of $S(q,\omega)$ were done. Unfortunately, the shape of $S(q,\omega)$ in this region is that of a featureless, monotonously decaying function, making comparison to theory difficult and demanding. It is known that the first region, $q/q_0 < 0.8$, represents a transition region from collective to single-atom motions, or if you like, from macroscopic to atomic scales. It is this region which is experimentally difficult to reach. The higher-q region displays more of single-atom motions. The present study is devoted mainly to this range, although some results derived from this q range are used for extrapolation to the small-q range by use of MD data. The aim is to gain a more detailed knowledge of atomic motions from $S(q,\omega)$ in this featureless range and to find more critical ways of investigation, not just by comparing $S(q,\omega)$ from theory with experiment.

During the last few years accurate measurements of $S(q,\omega)$ for some liquid metals were performed. The earlier result on liquid rubidium[7] was followed by accurate results on liquid lead[8] at 623 K and reasonably accurate results[8] at 1173 K as well as on liquid bismuth[9,10] at 578 K. As reported in a previous paper,[11] the intermediate scattering function $F(q,t)$ was also derived from the lead and bismuth measurements using an extrapolation technique to large-ω values as was used for the rubidium case:[12] a fit of a sum of three Gaussian functions to $S(q,\omega)$, which also gives an analytical form for its Fourier transforms $F(q,t)$. Knowing $F(q,t)$, one can derive numerically its memory functions of first order, $K(q,t)$, and second order, $M(q,t)$, by applying the Mori formalism. It was shown earlier[13] that $M(q,t)$ is closely related to $\Phi_l(q,t)$, which is the generalized time- and wavelength-dependent kinematic longitudinal viscosity, $\nu_l(q,t)$. As $\Phi_l(q,t)$ also plays the role of the time-dependent part of the memory function of the longitudinal current correlation function, its derivation from experimental data is already in itself of interest, as it can be compared to predictions from kinetic theory. The time integral of $\Phi_l(q,t)$ is also of considerable interest as it corresponds to $\nu_l(q)$, the wave-vector-dependent kinematical viscosity. This was recently computed for a hard-sphere system of various densities using MD.[2] A comparison of neutron and MD results for $\nu_l(q)$ can be made.

Furthermore, if the measured $S(q,\omega)$ are accurate

enough it is possible to derive the fourth-frequency moment $\langle\omega^4\rangle$, the value of which depends upon the pair interaction potential $V(r)$. A scheme for obtaining $V(r)$ from $\langle\omega^4\rangle$ was given a long time ago.[14] Knowing $\langle\omega^4\rangle$ from neutron experiments as well as the pair correlation function $g(r)$ and the structure factor $S(q)$ to a sufficient accuracy, one can derive $V(r)$ by a direct fit, as developed in this paper.

In the present article $\nu(q)$ is derived and compared to MD data for hard spheres. The neutron data on the memory functions for Pb at 623 and 1173 K, for Bi at 578 K, and Rb at 315 K serve as a calibration of the MD data. The general behavior of the $\nu(q)$ curve is traced This is reported in Sec. II.

With use of analytical form of pair potential with several free parameters, a form of $V(r)$ for liquid Pb at 623 K is derived. It is compared to other forms. In Sec. III we report the results.

Finally the form of the memory functions $\Phi_l(q,t)$ obtained from experiments is used to derive the short-time interaction part of the memory function for the longitudinal current correlation function, which can be directly compared to the corresponding result calculated from kinetic theory in its advanced mode-coupling version. This comparison is based upon the derived form of the interatomic potential for Pb at 623 K and upon other known potential data for Rb at 315 K. This is described in Sec. IV.

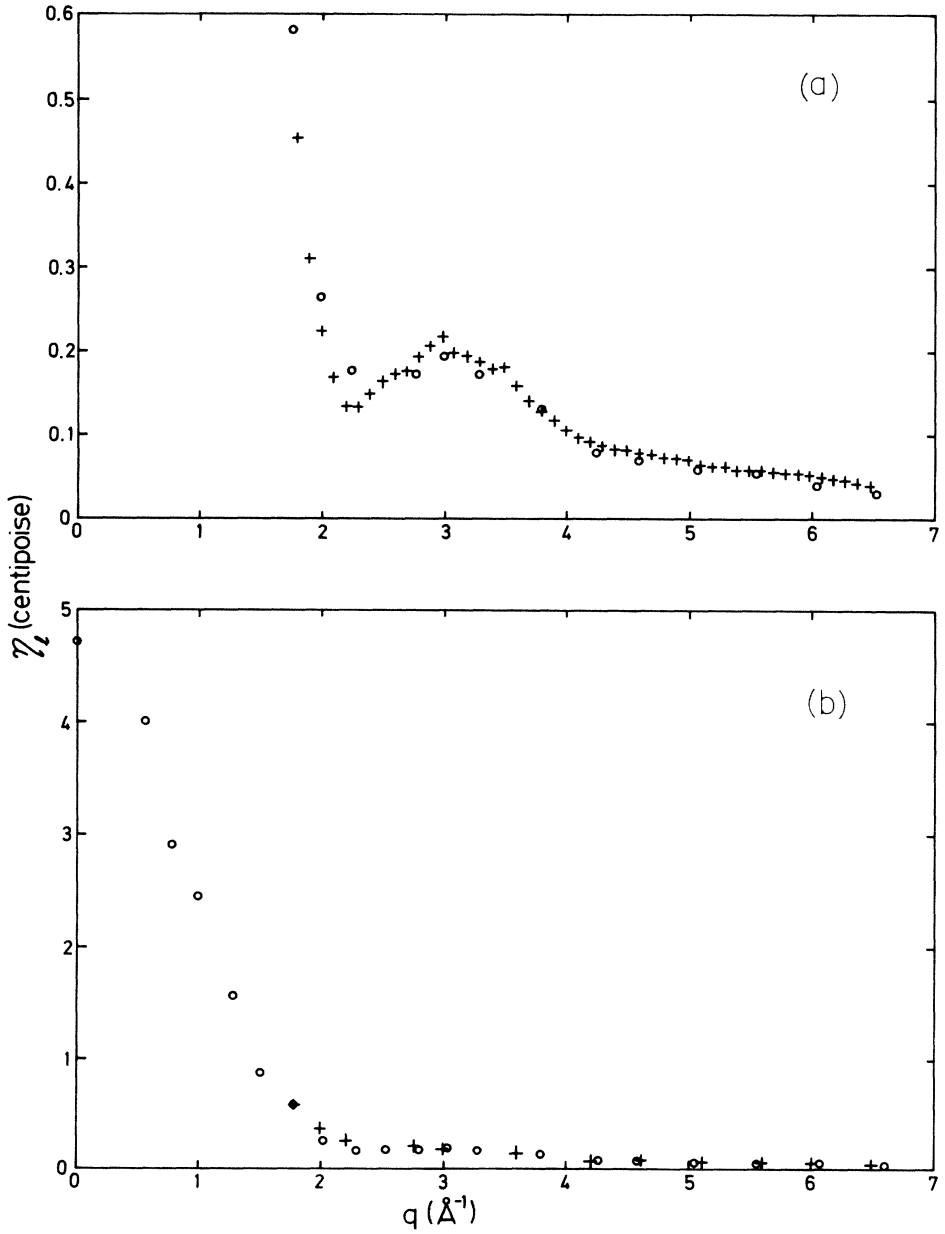

FIG. 1. Generalized viscosity $\eta_l(q)$ measured in centipoise, for liquid lead at 623 K. Neutron data (+); MD data (○). (a) q region of overlap between neutron and MD data for calibration of MD data. (b) Total q region including the calibrated MD data extrapolating $\eta_l(q)$ to $q=0$. $\eta_l(0)=4.85$ cP. Basic constants: $V/V_0=1.6$, $\sigma=3.0$ Å, $Mn=10.7$ g/cm^3.

II. GENERALIZED VISCOSITY FOR LIQUID Pb, Bi, AND Rb

The experimental basis for the following derivations of results is the availability of $F(q,t)$ from neutron scattering experiments at a large number of q values for all times and with sufficient accuracy. Such data exist for a number of liquid metals, namely[11,12] Pb at 623 and 1173 K, Bi at 578 K, and Rb at 315 K. These data are used in the present analysis.

The theoretical basis for the generalized viscosity follows from an application of the Mori memory-function formalism, first to $F(q,t)$, and then to its memory function $K(q,t)$, which, in turn, has its own memory function $M(q,t)$, and finally to the longitudinal current correlation function $J_l(q,t)$, which has its memory function $K_l(q,t)$. Due to the intimate relation between $F(q,t)$ and $J_l(q,t)$, which reads

$$J_l(q,t)=q^{-2}\frac{\partial^2 F(q,t)}{\partial t^2}\ , \tag{1}$$

it is easily established that[13]

$$M(q,t)=K_l(q,t)-\langle\omega^2\rangle/\langle\omega^0\rangle\ , \tag{2}$$

where $\langle\omega^0\rangle$ and $\langle\omega^2\rangle$ are the zeroth- and second-frequency moments of $S(q,\omega)$. From a generalization of hydrodynamics,[1] it may be shown that $K_l(q,t)$ can be expressed as follows,

$$K_l(q,t)=\langle\omega^2\rangle/\langle\omega^0\rangle+q^2\Phi_l(q,t)\ , \tag{3}$$

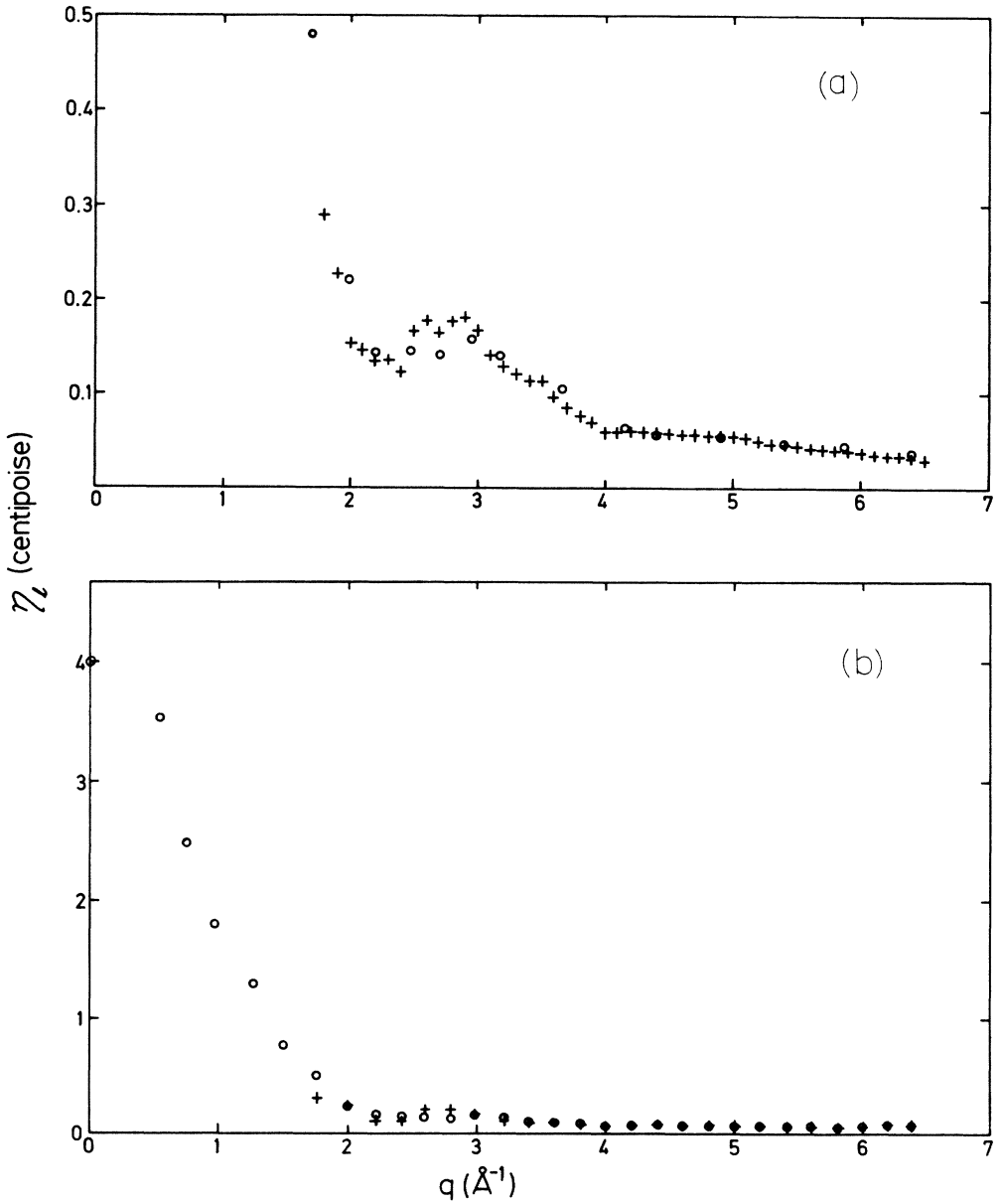

FIG. 2. Generalized viscosity $\eta_l(q)$ measured in centipoise for liquid bismuth at 578 K. Notation same as in Fig. 1. $\eta_l(0)=4.0$ cP. Basic constants: $V/V_0=1.6$, $\sigma=3.1$ Å, $Mn=10.03$ g/cm^3.

where $\Phi_l(q,t)=\nu_l(q,t)$ is the generalized longitudinal kinematic viscosity. In the macroscopic limit,

$$\nu_l=(1/Mn)(\tfrac{4}{3}\eta_s+\eta_v)=\eta_l/Mn \ ,$$

where η_s and η_v are the shear and volume viscosity, respectively, M is the atomic mass, and n is the number density. From (2) and (3) is is seen that

$$\nu_l(q,t)=(1/q^2)M(q,t) \ . \tag{4}$$

Of primary interest for the present purposes is the time integral of (4), which is equivalent with the $\omega=0$ value of its Fourier transform $\tilde{\nu}_l(q,\omega)$:

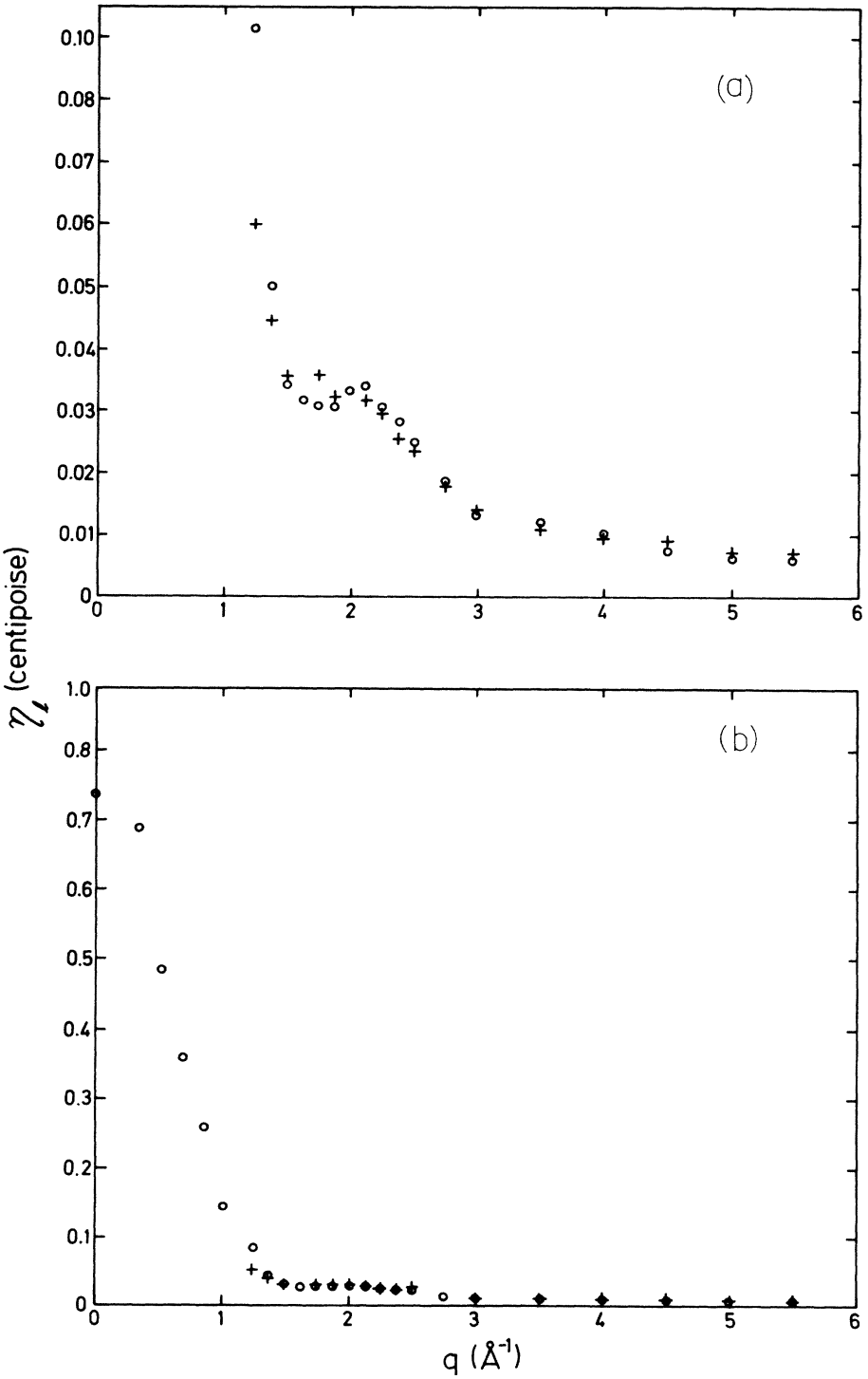

FIG. 3. Generalized viscosity $\eta_l(q)$ measured on centipoise for liquid rubidium at 315 K. Notation same as in Fig. 1. $\eta_l(0)=0.74$ cP. Basic constants: $V/V_0=1.6$, $\sigma=4.4$ Å, $Mn=1.481$ g/cm^3.

$$\tilde{\nu}_l(q)=\lim_{\omega\to 0}\int_0^\infty \nu_l(q,t)\cos(\omega t)dt\ . \tag{5}$$

This quantity was computed with MD methods by Alley and Alder[2] within the formalism of generalized linear hydrodynamics for hard spheres. The idea behind that procedure is to keep the ordinary hydrodynamical equations unchanged down to atomic dimensions. The transport coefficients are, however, as a consequence, assumed to be wave-vector and time dependent and are calculated from the appropriate correlation functions calculated numerically with MD. In what follows, MD data are compared to the neutron data. The MD data are fitted to the neutron data over the q region studied in the neutron experiments. This region is $0.8<q/q_0<3$ for Pb and Bi and $0.8<q/q_0<3.7$ for Rb. About fifty constant-q cuts in the $S(q,\omega)$ surface were used for Pb and Bi. As the MD data are given down to small-q values and are normalized to the value at $q=0$, these data, thus normalized by the absolute neutron data, are used to find the value of $\nu_l(q)$ for $q=0$. The MD data exist for different packing fractions V/V_0: 1.6, 3.0, and 10. For Pb at 623 K, Bi at 578 K, and Rb at 315 K, the value of V/V_0 is close to 1.6. For Pb at 1173 K it is close to 2.0. For this case an interpolation between the MD data at 1.6 and 3.0 was used to obtain the MD shape of the curve $\nu(q)$ [this is called $\alpha(k)/\alpha(0)$ in the paper of Alley and Alder; compare the last column in Tables I and II in Ref. 2]. The value of V/V_0 is calculated from

$$\frac{V}{V_0}=\frac{\sqrt{2}}{n\sigma^3}\ , \tag{6}$$

where n is the number density and σ is the atomic radius. This is taken at 3.0 Å for Pb, 3.1 Å for Bi, and 4.4 Å for Rb.

The result for Pb at 623 K is shown in Figs. 1(a) and 1(b). The experimental values of $\nu(q)$ have in this and all

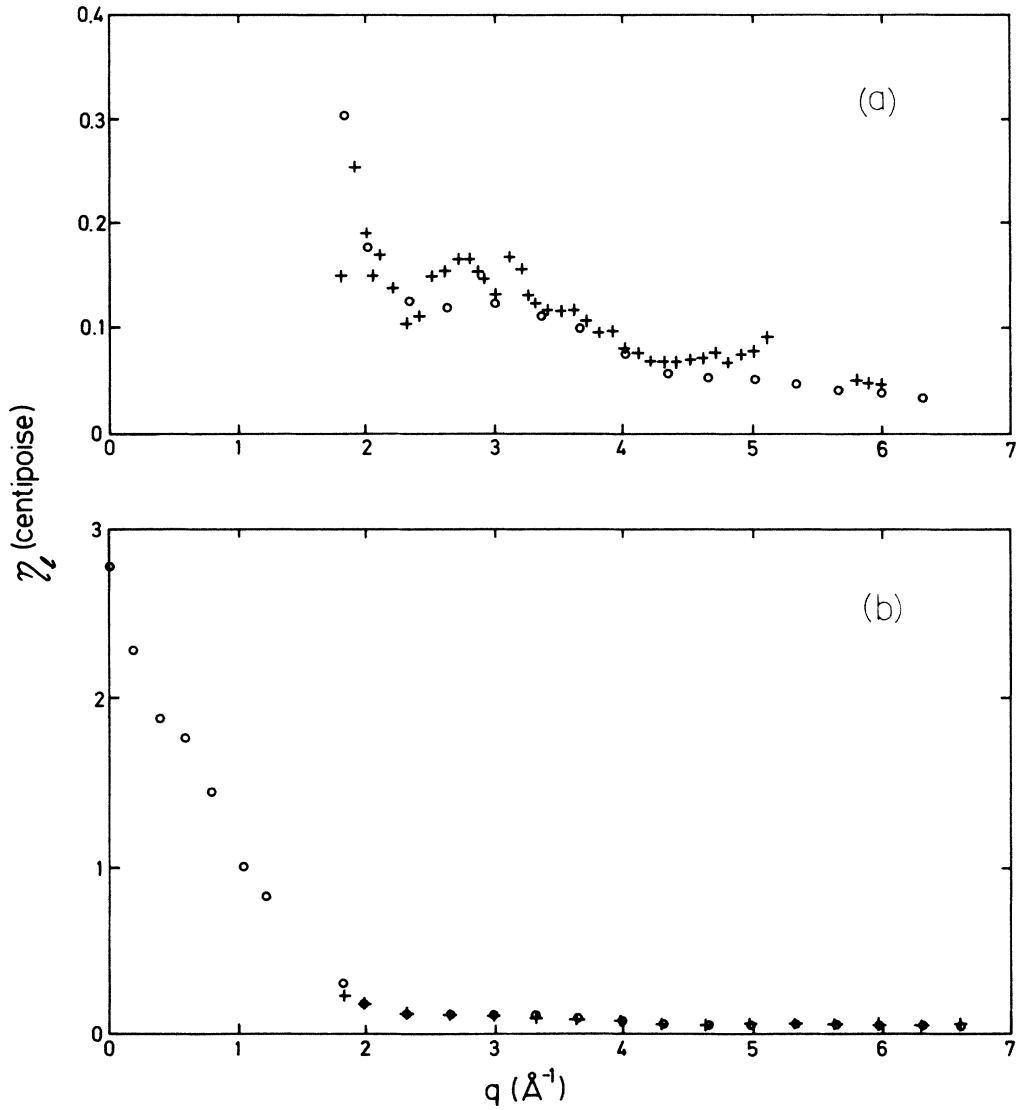

FIG. 4. Generalized viscosity $\eta_l(q)$ measured in centipoise for liquid lead at 1173 K. Notation same as in Fig. 1. $\eta_l(0)=2.8$ cP. Basic constants: $V/V_0=2.0$, $\sigma=3.0$ Å, $Mn=9.146$ g/cm^3.

subsequent figures been multiplied with Mn, where M is the atomic mass, to obtain $\eta_l(q)$, here given in centipoise. $\eta_l(q)$ from neutron scattering measurements is seen to be influenced by the liquid structure [Fig. 1(a)], showing a minimum at $q=q_0$ (2.2 Å^{-1}). It is also seen that the MD data show a similar tendency, and, on the whole, the agreement in shape is remarkable. When the entire q range is plotted as done in Fig. 1(b), it is observed that the change from atomic towards macroscopic behavior sets in at q values just below q_0. For $0<q/q_0<0.9$ the value of $\eta_l(q)$ changes from approximately 0.15 cP at $0.9q_0$ to 4.8 cP at $q=0$. In just this region ($0<q/q_0<0.9$) the two components $S_s(q,\omega)$ and $S_d(q,\omega)$, where the indices d stands for distinct and S_d describes the pair motions, tend to balance each other and thus give a very low value of $S(q,\omega)$, making it very difficult to study this function experimentally.

The macroscopic value from direct measurements of η_s and η_v is 4.4 cP. An estimation of η_l from formulas given in Faber's book on liquid metals[15] give $\eta_s=0.025$ P and with $\eta_v\cong 0.3\eta_s$ the value of $\frac{4}{3}\eta_s+\eta_v$ is 4.0 cP. It is observed that the macroscopic values and extrapolated neutron data agree within 10% or 20%.

In Figs. 2(a) and 2(b) the corresponding comparison is made between the bismuth results from neutron scattering and MD data. Again it is observed [Fig. 2(a)] that MD data show the same shape as the neutron data ($q_0=2.2$ Å). When extrapolated to $q=0$ with the aid of calibrated MD data, the value obtained is 4.0 cP. Flinn[16] found, in ultrasound studies, $\eta_s=1.62$ cP and $\eta_v=7.7$ cP, which adds up to $\eta_l=\frac{4}{3}\eta_s+\eta_v=9.9$ cP. Use of the formulas given in Faber's book give $\eta_s=2.2$ cP and $\eta_l\cong 3.0+\eta_v$. The final result depends upon the value of η_v. If one accepts Flinn's value, one obtains $\eta_l=10.7$ cP. If, on the other hand, the value of η_v is of order $0.3\eta_s$, the value would be 3.7 cP. The relatively large discrepancy between the extrapolated neutron value of 4.0 cP and the macroscopic values 9.9 or 10.7 cP seems to depend upon the large macroscopic value of η_v, 7.7 cP.

In Figs. 3(a) and 3(b) the rubidium neutron data are used for normalization of the MD data. Again there is a remarkable, detailed shape agreement in the high-q range $0.8<q/q_0<3.5$ [Fig. 3(a); $q_0=1.5$ Å]. The extrapolation to $q=0$ by use of the calibrated MD curve gives $\eta_l(0)=0.74$ cP. The experimental value for η_s is 0.64 and 0.59 cP from a MD simulation study.[17] If we assume 0.6 cP, the value of $\eta_l=0.8+\eta_v$, giving a total of the order of 1 cP (η_v unknown, but assumed $=0.3\eta_s$). We notice that the present neutron value is in the same region of values within 25%.

In Figs. 4(a) and 4(b), finally, the high-temperature lead (1173 K) neutron data are used for calibration of the MD data. The quality of the neutron data are much worse here due to background difficulties, but the general shape remains in agreement. The $\eta_l(0)$ value comes out as 2.8 cP. No macroscopic experimental data exist for this high temperature. Flinn's data range from the melting point at 600 K up to 925 K. The trend of her data is such that η_s decreases roughly exponentially with temperature and η_v increases exponentially. If these trends are extrapolated up to 1173 K, one finds $\eta_s=0.87$ cP and $\eta_v=17.5$ cP, giving $\eta(0)=18.4$ cP. There is, however, a tendency of increasing η_s and decreasing η_v for the last two viscosity values at 875 and 925 K in her data. The value of $\eta_l(0)$ is therefore uncertain. It seems that $\eta_v(0)$ is much too high to result in the $\eta_l(0)=2.8$ cP value found from neutron-MD data.

The low-temperature data at $V/V_0=1.6$ all show similar behavior. The reason that the value of $\eta_l(0)$ for rubidium differs ($=0.74$ cP) from those of lead ($=4.8$ cP) and bismuth ($=4.0$ cP) by a factor of 6 is that the value of the density, Mn, differs by the same factor. It is then of interest to compare $\nu_l(q)$ for the different liquids when the factor Mn is divided out. Also the structure effects should be removed, which is done by comparing $\nu_l(q/q_0)$ for various liquid metals. In Fig. 5 the three liquids are compared. It is seen that all results fall within a relatively narrow band. This is made even more evident in Fig. 6, in which the entire range down to $q=0$ of $\nu_l(q/q_0)$ is plotted for the three liquids. It seems that the relative differences are small. The main difference in viscosity, $\eta_l(q)$, is created by the density values.

To sum up the results of this section, we find the following characteristics.

(a) The various liquid metals show about the same reduced variation of ν_l as a function of q/q_0. The absolute values of $\eta_l(q)$ are to a large extent determined by the liquid density and its structure.

(b) The shape of the viscosity curves $\nu_l(q)$ derived from MD within the framework of generalized hydrodynamics shows a remarkable agreement with $\nu_l(q)$ from neutron scattering data. A similar statement applies for the data obtained by Ailawadi, Rahman, and Zwanzig[1] on an argonlike system.

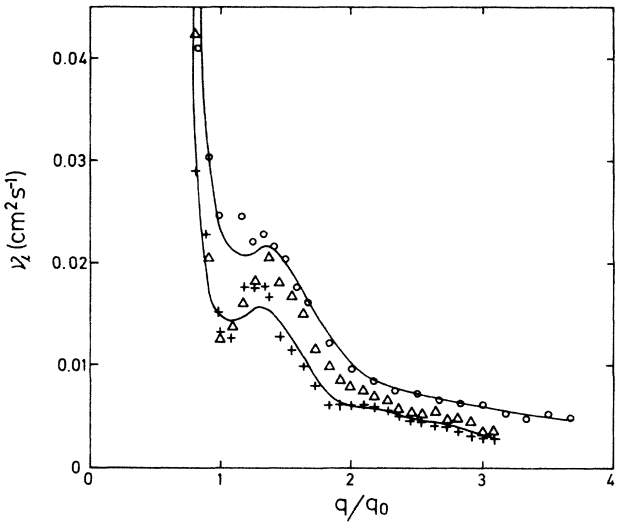

FIG. 5. Generalized kinematic viscosity ν_l as a function of reduced q/q_0 derived from neutron data on liquid Bi at 578 K, Pb at 623 K, and Rb at 315 K in the large-wave-vector region, $0.8<q/q_0<3.7$. Bi data (+); Pb data (△); Rb data (○). MD data fitted to Bi and Rb neutron data (solid line). It should be noted that $\eta_l(q)=Mn\times 10^{-2}\int_0^\infty \Phi_l(q,t)dt$ cP and $\Phi_l(q,t)=(1/q^2)(\langle\omega^4\rangle/\langle\omega^2\rangle-\langle\omega^2\rangle/\langle\omega^0\rangle)n(q,t)$, where $n(q,t)=\Phi_l(q,t)/\Phi_l(q,0)$. $\nu_l(q)=\eta_l(q)/Mn$.

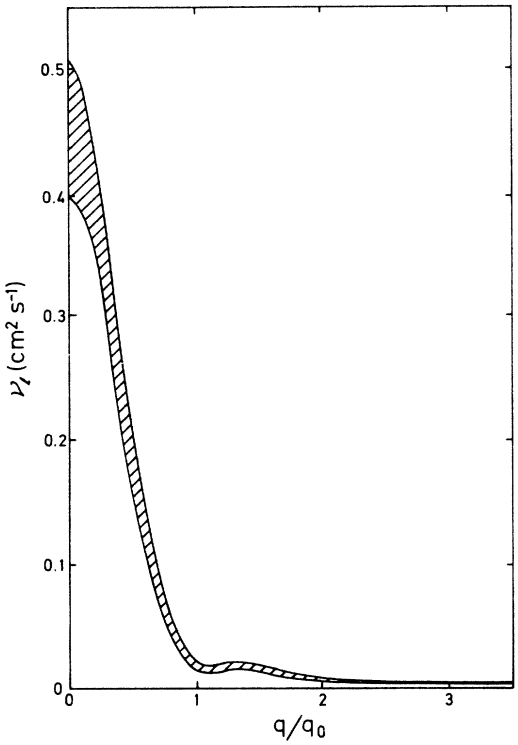

FIG. 6. Band (shaded area) of values of generalized kinematic viscosity, $\nu_l(q/q_0)$, within which the neutron observed values for liquid Bi at 578 K, Pb at 623 K, and Rb at 315 K fall in the large-q range, $0.8 < q/q_0 < 3.7$, and would fall also in the small-q range, $0 < q/q_0 < 0.8$, if the hard-sphere MD data would give a good result in this range. The lower limiting curve is fitted MD data for liquid Bi and the upper limiting curve is fitted MD data for liquid Rb. The fitted MD data for liquid Pb falls in between these two curves. Fitted limiting MD curves (solid line).

(c) The extrapolated values at $q=0$ for the viscosities come out with the correct magnitude, in some cases even quantitatively correct within 10% to 20% from the macroscopic values. These latter values are in some cases dubious or unknown. In particular, the values of η_v seem to be of determining importance. The observed discrepancies could be due to incorrect values of η_v. It could also depend upon a failure of the hard-sphere-model concept at small-q values. This could be particularly true for bismuth, in which directional nonspherical forms of atomic potentials may be of importance.

(d) As the MD data are based on the hard-sphere assumption, we are, however, forced to the conclusion that the interatomic potentials do not seem to play a very large role in the small-wavelength range $q/q_0 > 0.9$. A possible exception may be the role of $\eta_v(q)$ as discussed above. Possibly the potential shape plays a role for $q/q_0 < 0.9$ and particularly for $q \to 0$.

(e) The mathematical framework of generalized linear hydrodynamics seems to work remarkably well in spite of the many potential difficulties such as failure of the linear approximation and the fact that for $q/q_0 > 1$ $S(q,\omega)$ is dominated by $S_s(q,\omega)$. What is the meaning of hydrodynamics for self-motion? What little is left of collective behavior as manifested in a very small $S_d(q,\omega)$ may be sufficient to motivate the use of hydrodynamic concepts [compare the shape of the memory function $\Gamma_{11}(q,t)$ discussed in Sec. IV]. If this generalized form of hydrodynamics is recast into a viscoelastic theory, the conceptual difficulties may seem to disappear.

III. INTERATOMIC POTENTIAL FOR LIQUID Pb AT 623 K FROM FOURTH-FREQUENCY MOMENT

The mathematical form for the fourth-frequency moment is well known,

$$\frac{\langle\omega^4\rangle}{\langle\omega^2\rangle} = \langle\omega_l^2\rangle = 3q^2v^2 + \Omega_0^2 - \Omega_q^2 , \tag{7}$$

where $\langle\omega_l^2\rangle$ is the second-frequency moment of longitudinal current correlation, $v^2 = k_B T/M$,

$$\Omega_0^2 = \frac{4\pi n}{3M}\int_0^\infty r^2 dr\, g(r)\left[V''(r) + \frac{2V'(r)}{r}\right],$$
$$\Omega_q^2 = \frac{4\pi n}{M}\int_0^\infty r^2 dr\, g(r)\left[V''\left[\frac{\sin(qr)}{qr} + \frac{2\cos(qr)}{(qr)^2} - \frac{2\sin(qr)}{(qr)^3}\right] - \frac{2V'}{r}\left[\frac{\cos(qr)}{(qr)^2} - \frac{\sin(qr)}{(qr)^3}\right]\right]. \tag{8}$$

$3q^2v^2$ is a kinematic, free-motion term which we subtract, and Ω_0^2 is the characteristic frequency, or let us say, the Einstein frequency of the system.

The quantity $\langle\omega_l^2\rangle - 3q^2v^2$ oscillates around the value Ω_0^2 due to the oscillatory term in Ω_q^2. It is characterized by the amplitude of oscillation as well as the period. We expect that both properties are sensitive to the choice of $V(r)$.

Our method to get a pair potential out of the $S(q,\omega)$ data is the following.

First, the $S(q,\omega)$, $\omega^2 S(q,\omega)$, and $\omega^4 S(q,\omega)$ curves obtained from the fitting of a sum of three Gaussians to $S(q,\omega)$ are carefully inspected for the larger ω values for all of the 50 q cuts in $S(q,\omega)$, which are used in this analysis. For about one-third of the data it is observed that the last few values of $\omega^2 S(q,\omega)$ for the largest ω values deviate markedly from the fitted curve. This is due to incomplete corrections for multiple scattering. These points are discarded. Then a new least-squares fit is now made to $\omega^4 S(q,\omega)$. Even in the worst cases the new fit differs little from the first fit. The analytical forms for $S(q,\omega)$ were Fourier-transformed and the resolution—

assumed to have a Gaussian form—removed to obtain $F(q,t)$. The moments $\langle\omega^2\rangle$ and $\langle\omega^4\rangle$ were then obtained from the appropriate derivatives at $t=0$. Then $\langle\omega^4\rangle/\langle\omega^2\rangle-3q^2v^2$ is plotted for the 50 q values. This is the raw material for our potential fit.

For the potential shape we test a variety of cases fitting the calculated $\Omega_0^2-\Omega_q^2$ to $\langle\omega^4\rangle/\langle\omega^2\rangle-3q^2v^2$. From discussion in the literature it is probable that the potential for lead should have a shape of the type found by Johnson, Hutchinson, and March,[18] later tested and discussed by Schiff[19] and by Jacobs and Andersen.[20] After some preliminary test calculations we adopted the following potential shape:

$$V_1(r)=B\left[1+C\left[\frac{r_m}{r}\right]^n\right]\left[\frac{|r-r_m|}{r_m}\right]^2 -D\left[\frac{|r-r_m|}{r_m}\right]^3+E,\quad r\le r_m$$
$$V_2(r)=\frac{A}{r^3}\cos[2k(r+\beta)]e^{-\alpha r},\quad r>r_m\ . \tag{9}$$

This potential contains ten free parameters, of which four are eliminated, however, if we require that at $r=r_m$ (the potential minimum) we have

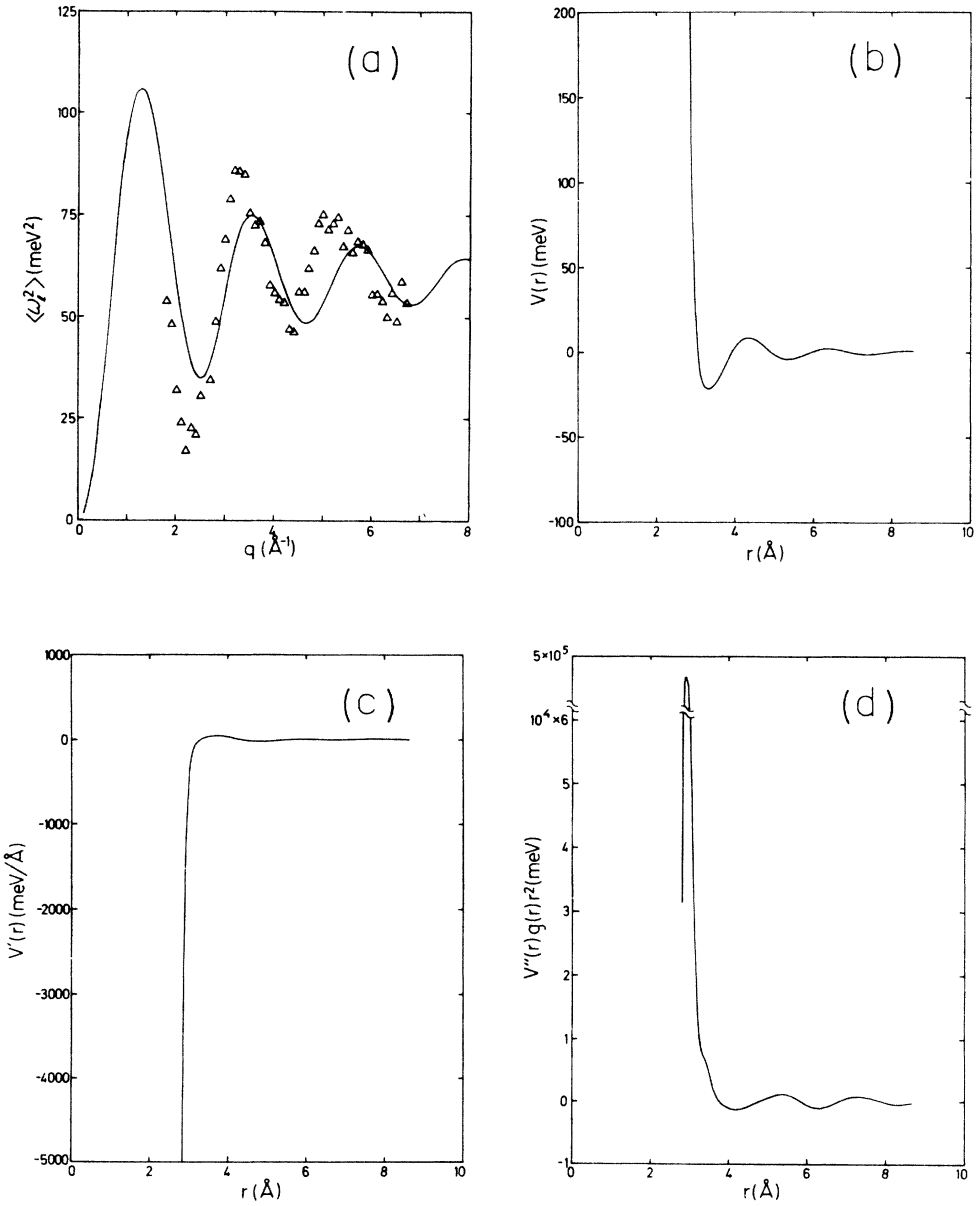

FIG. 7. Fit of the potential form at Eq. (9) to observed fourth moment for liquid Pb at 623 K. $n=25$ (strongly repulsive potential). (a) Result of fit (solid line); experimental points (△). (b) Resulting potential. (c) Force, $V'(r)$. (d) Integrand, $V''(r)g(r)r^2$.

$$V_1(r_m)=V_2(r_m),\quad V_1'(r_m)=V_2'(r_m)\ ,$$
$$V_1''(r_m)=V_2''(r_m),\quad V_1'''(r_m)=V_2'''(r_m)\ . \tag{9'}$$

These requirements are necessary to obtain a smooth variation of the integrands in Ω_0^2 and Ω_q^2 in Eq. (8).

The potential defined from Eq. (9) contains a repulsive part, whose steepness can be varied as r^{-n}. It also contains a harmonic as well as an anharmonic term in $V_1(r)$. $V_2(r)$ contains well-known Friedel oscillations determined by a "Fermi-surface" wave vector $\mathbf{k}$.

In addition to the potential $V_1(r)+V_2(r)$, we also tested the repulsive part $V_1(r)$ for $r<r_m$ only. As the results seemed insensitive to the shape of the attractive part $V_2(r)$, we also tried a nonoscillatory form of the Lennard-Jones (LJ) type,

$$V(r)=4\epsilon[(\sigma/r)^{12}-(\sigma/r)^6]\ .$$

Our final fittings were performed for four different powers n of the r^{-n} term in $V_1(r)$, namely from a very steep potential with $n=25$, through $n=12$, where we also tested the Lennard-Jones shape for comparison, $n=8$, and finally to $n=5$, the softest potential tried. Parameters for the various fittings are given in Table I. Regarding the parameters of the potential, the following is noted: The potential minimum position—r_m—changes very little with power n as well as with the value of the $\mathbf{k}$ vector. As a consequence, the phase factor β also varies very little. The "Fermi-surface" width factor α seems to be constant for these potential choices. The most significant changes occur in the potential depth.

In Figs. 7–9 we give the results of the fittings for the

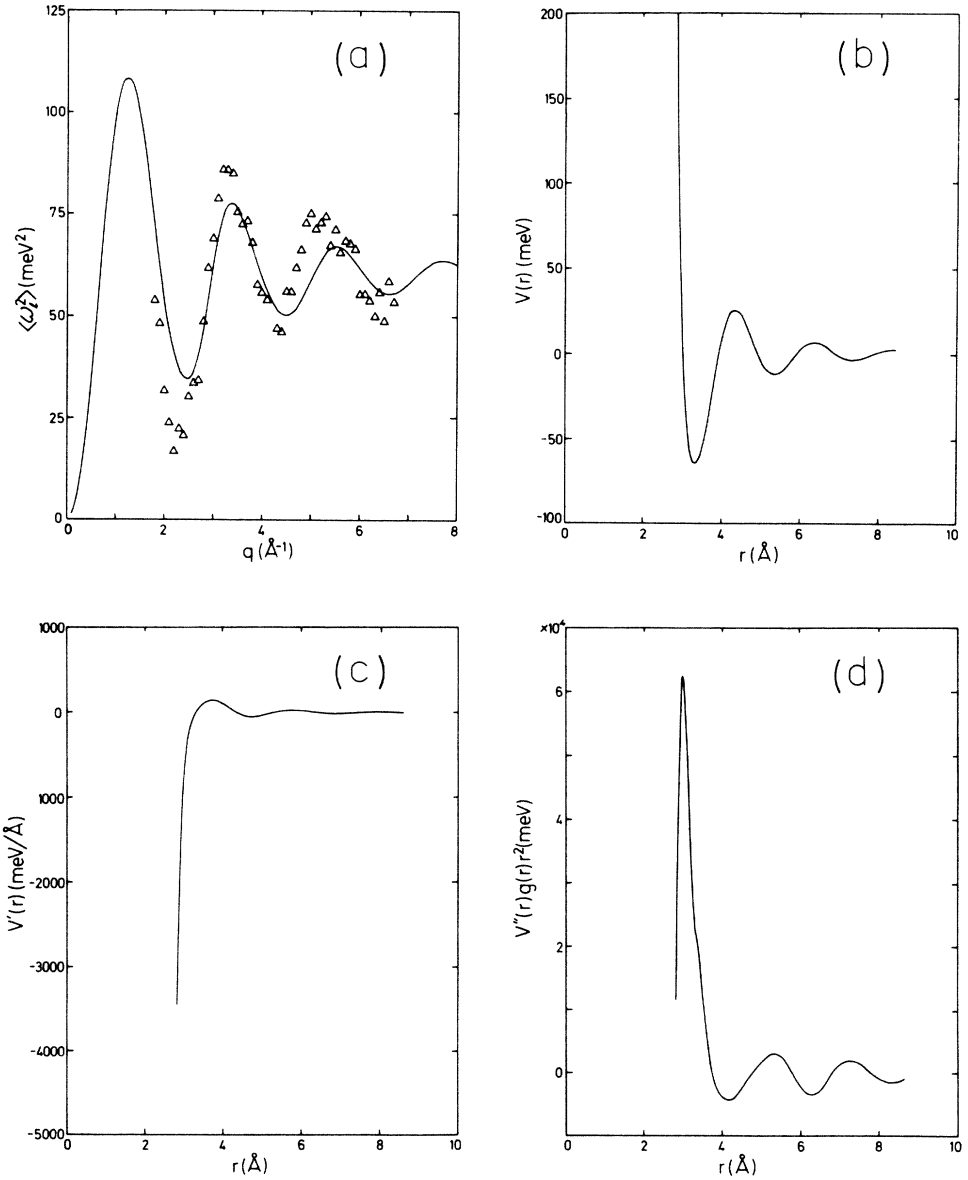

FIG. 8. Fit of the potential form at Eq. (9) to observed fourth moment for liquid Pb at 623 K. $n=12$ (medium strong repulsive potential). (a)–(d) Same as in Fig. 7.

TABLE I. Parameters of the potential given by Eq. (9) for different powers of its repulsive part.

n	B (meV)	C	D (meV)	E (meV)	r_m (Å)	A (meV Å^3)	$2k$ (Å^{-1})	β (Å)	α (Å^{-1})
5	1048.0	5.32	12 620	−93.3	3.37	5564.0	3.43	−2.54	0.12
8	964.4	5.06	25 500	−102.0	3.33	5927.0	3.09	−2.41	0.12
12	971.5	2.92	25 260	−64.6	3.32	3711.0	3.15	−2.42	0.12
25	977.6	0.31	4624	−21.6	3.33	1250.0	3.15	−2.43	0.12

Lennard-Jones potential $\sigma = 3.02$ Å $\epsilon = -100$ meV

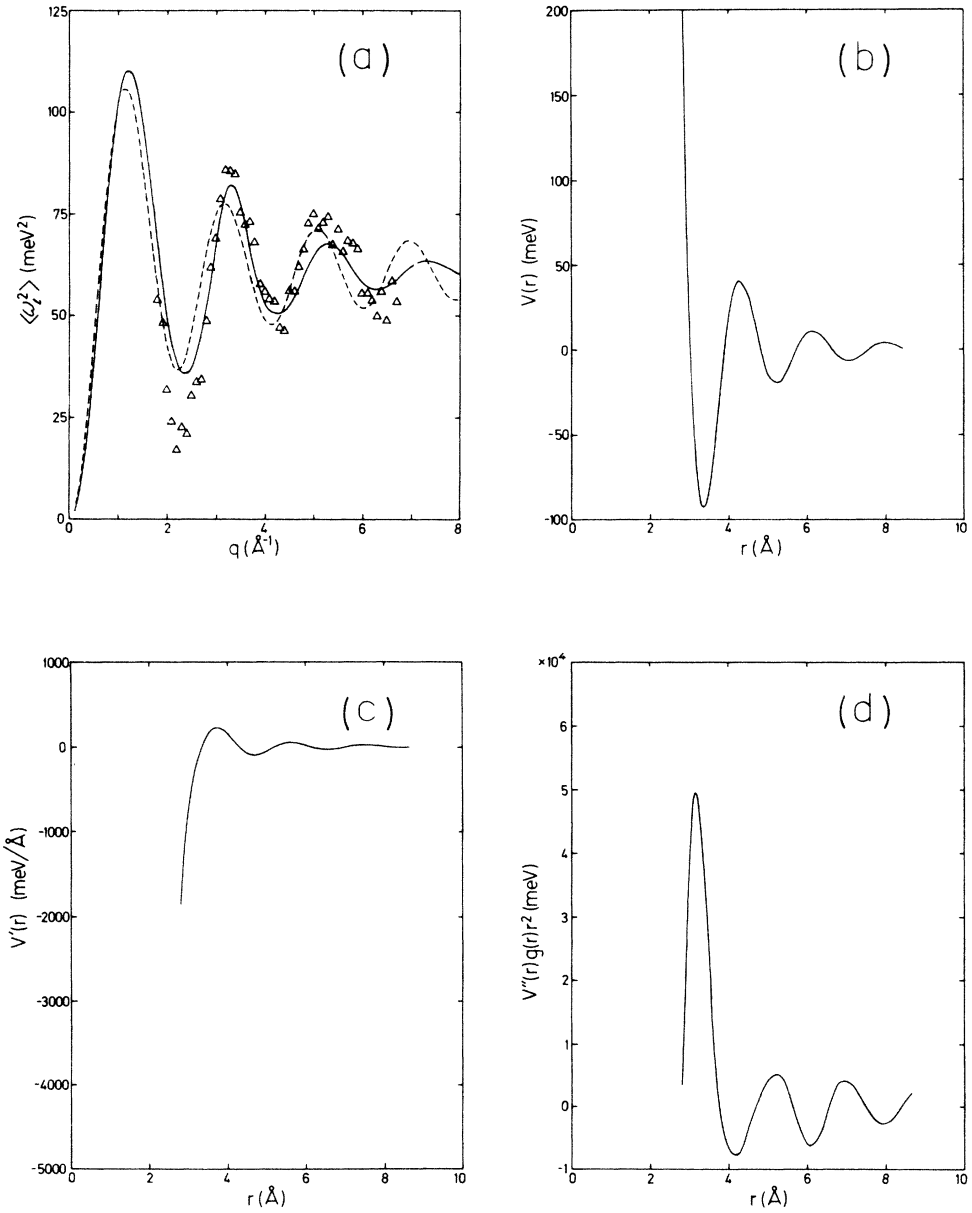

FIG. 9. Fit of the potential form at Eq. (9) to observed fourth moment for liquid Pb at 623 K. $n = 5$ (soft core, weaker repulsion). (a)—(d) Same as in Fig. 7. Equation (10) fitted to the data (dashed line).

various powers n. The figures also include the potential, its first derivative (the force), and the integrand $V''(r)g(r)r^2$ in Eq. (8) for Ω_0^2 and Ω_q^2. It is seen that the periodicity of the fitted fourth moment, $\Omega_0^2-\Omega_q^2$, is sensitive to the n value, the best fit occurring at $n=5$. Going from $n=25$ to $n=5$ the potential changes rather dramatically from a shallow one to a deep one with a slightly-higher-frequency Friedel oscillation. In all cases it is found that the attractive force for $r>r_m$ is very small compared to the very large repulsive one. It is also observed that the variation of the repulsive force with power n is not too dramatic, making the fitting procedure relatively insensitive.

Finally, in the integrals defining Ω_0^2 and Ω_q^2 the factor $V''(r)g(r)r^2$ is in all cases strongly peaked at a particular value of r, which varies from 2.8 to 3.1 Å. The value of the integral defining Ω_0^2 is, to 90% or more, determined by this large peak. The contribution from the attractive part shows cancellation effects due to the Friedel oscillations. This fact is the reason why an approximate form of $\langle\omega^2\rangle$ is often successfully used, namely

$$\Omega_0^2-\Omega_q^2=\omega_E^2\left[1-\frac{3\sin(qr_0)}{qr_0}-\frac{6\cos(qr_0)}{(qr_0)^2}+\frac{6\sin(qr_0)}{(qr_0)^3}\right], \tag{10}$$

where ω_E^2 stands for a somewhat simplified version of Ω_0^2, namely neglecting the term $V'(r)$. This approximation with $\omega_E=7.60$ meV and $r_0=3.3$ Å is also given as a dashed line in Fig. 9 in the plot of $\Omega_0^2-\Omega_q^2$ (upper left-hand corner). It fits the experimental fourth moment relatively well, but not as well as Eq. (9) does with the set of

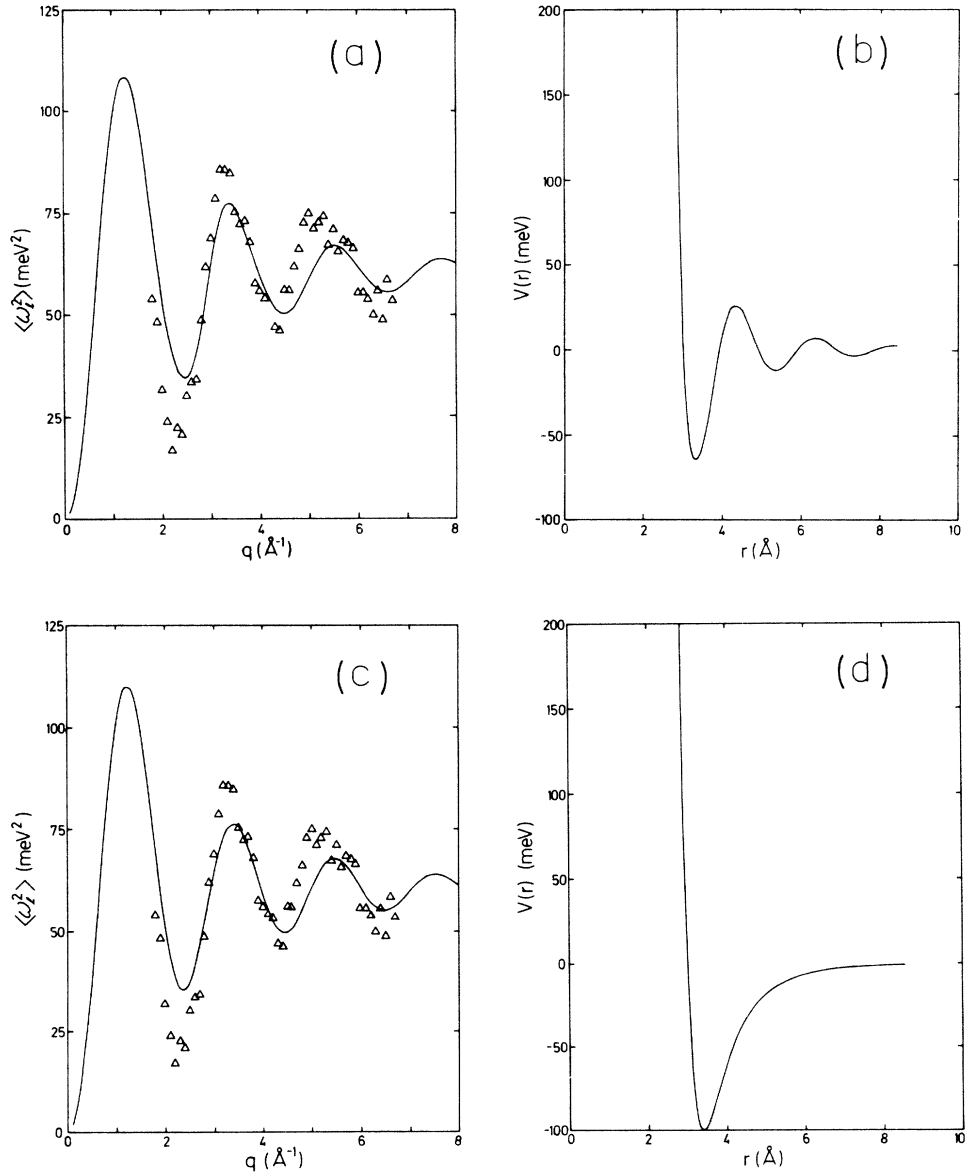

FIG. 10. Comparison of fit of the potential form of Eq. (9) with $n=12$ and Lennard-Jones potential for liquid Pb at 623 K. (a) Result of fit with potential according to (b). (c) Result of fit with potential according to (d).

parameters belonging to the $n=5$ case.

In Fig. 10 a LJ potential with $\sigma=3.02$ Å was compared to the Jacobs type with $n=12$. The depth—$\epsilon=-100$ meV—of the LJ potential came out identical to the energy difference between the first maximum and minimum of the fitted Jacobs type [Eq. (9)]. It is observed that the two calculated fourth moments are indistinguishable. The conclusion is that the attractive part cannot be determined with confidence from fittings in this large q range $q/q_0>0.9$, a fact discussed in the literature.

In addition, use of only the repulsive part $V_1(r)$ of the potential to a large extent verifies that the attractive part plays a very minor role here, if any at all.

In summation, we conclude that the best fit for the liquid lead at 623 K is characterized by a soft core defined by the r^{-5} repulsion (Table I).

We notice that the zero-sound or Brillouin peaks were observed in liquid lead at 623 K up to approximately $q/q_0<\frac{2}{3}$. A similar soft potential and extension of zero-sound peaks were also observed in liquid rubidium. This is to be contrasted to liquid argon with its steeper potential and its shorter range for zero-sound peaks. On the other hand, this result seems to be in contradiction with the success of the hard-sphere model in predicting correct shape of the viscosity function $\nu(q)$ introduced in the preceding section. The explanation probably is that $\nu(q)$ function is too insensitive for potential details to show up, possibly only when $q\to 0$. In the $\nu(q)$ case the degree of packing seems more important.

IV. MEMORY FUNCTIONS FOR LONGITUDINAL CURRENT CORRELATION. LIQUID Pb AND Rb

The last aim of this paper is to establish a connection between the memory functions $\Phi_l(q,t)$ derived from neutron scattering for the longitudinal current correlation function (time-dependent part) and the prediction of kinetic theory. In Sec. II we were interested in its time integral $[=\nu(q)]$. Now we shall look somewhat into its detailed time dependence. This is characterized by an initial rapidly decaying part followed by an oscillatory tail. If we want to facilitate comparison with predictions from modern kinetic theory in the mode-coupling version, we find that in the calculations performed so far—mostly limited to the small-q region, $q/q_0<0.8$, the formulated memory functions contain just the same features—a rapidly decaying initial part approximated with a Gaussian function, followed by a complicated tail determined by various mode-coupling integrals. The Gaussian-shaped part is described as containing the physics of the binary collision plus the first rapid atomic rearrangements in the neighborhood of the collision site. This is the caging phenomenon. Considering the fact that this study is performed in a large-q range in which the Gaussian part dominates—at least in $\Phi_l(q,t)$—we limit our analysis to the short-time range. This does not mean that the longer-time tail is absent or unimportant. Its theoretical treatment is more complicated and its analysis is therefore left for future work.

At first we have to establish a relation between the memory function derived from kinetic theory and the function $K_l(q,z)$ [Laplace transform of $K_l(q,t)$ obtained from neutron experiments mentioned above], which is

$$K_l(q,z)=\frac{q^2v^2}{S(q)}\frac{1}{z}+q^2\tilde{\Phi}_l(q,z)\ . \tag{11}$$

According to Sjögren,[5(c)] the longitudinal current correlation is

$$C_l(q,z)=\frac{C_l^s(q,z)}{1-[(q^2v^2/z)nc(q)-\Gamma_{11}^d(q,z)]C_l^s(q,z)}\ . \tag{12}$$

In agreement with the formulation of Sjögren and Sjölander, we write, for the self-current-correlation $C_l^s(q,z)$,

$$C_l^s(q,z)=\frac{C_l^0(q,z)}{1+\Gamma_{11}^s(q,z)C_l^0(q,z)}\ , \tag{13}$$

where the free-atomic-motion current correlation $C_l^0(q,z)$ follows from (see Boon and Yip,[21] pp. 188–192, specialized to the noninteraction case)

$$C_l^0(q,z)=\frac{1}{z+q^2v^2/z+\Gamma^0(q,z)}\ . \tag{14}$$

Here, $\Gamma_{11}^d(q,z)$ and $\Gamma_{11}^s(q,z)$ are, respectively, the memory functions for the distinct and self-parts of the longitudinal current correlations. We notice that the free-motion part is separated out from $\Gamma_{11}^s(q,z)$ and contained in $\Gamma_0(q,z)$, $nc(q)=1-[S(q)]^{-1}$. Substituting Eqs. (14) and (13) into (12), one finds

$$\begin{aligned}C_l(q,z)&=\frac{1}{z+(q^2v^2/z)[1-nc(q)]+\Gamma_{11}(q,z)+\Gamma^0(q,z)}\\&=\frac{1}{z+K_l(q,z)}\ .\end{aligned} \tag{15}$$

Here,

$$\Gamma_{11}(q,z)=\Gamma_{11}^s(q,z)+\Gamma_{11}^d(q,z)\ ,$$

i.e., the memory function for the total longitudinal current correlation decreased by the free-motion memory function and the term $[q^2v^2/S(q)](1/z)$.

Now the two memory functions in Eqs. (11) and (15) must be the same, giving

$$\Gamma_{11}(q,z)=q^2\Phi_l(q,z)-\Gamma^0(q,z)\ . \tag{16}$$

If we now want to concentrate on the Gaussian binary collision part of Γ_{11}, which is denoted $\Gamma_{11}^B(q,z)$, this is easily done. Our procedure is now the following:

We have, directly from the neutron studies, the function $q^2\Phi_l(q,t)$. We write the Mori equation (14) for the free gas and solve it numerically to obtain $\Gamma^0(q,t)$. This is subtracted from $q^2\Phi_l(q,t)$. According to Eq. (16), we then compare the result thus obtained with $\Gamma_{11}(q,t)$, which we can calculate from Sjögren's kinetic theory. It is in this last phase of the analysis that we limit ourselves to the calculation of $\Gamma_{11}^B(q,t)$. Γ_{11}^B is given by

$$\Gamma_{11}^{B}(q,t)=\left[\frac{\langle\omega^4\rangle}{\langle\omega^2\rangle}-3q^2v^2+q^2v^2nc(q)\right]\times\exp\left[-\frac{t^2}{[\tau_l(q)]^2}\right]. \tag{17}$$

The width function $\tau_l(q)^{-2}$ is determined from theory. Its calculation is already rather lengthy. From Sjögren's results it is clear that one can at first calculate the self-part $[\tau_l^s(q)]^{-2}$ and compare it to the derived width function from the neutron data [compare Sjögren, Ref. 5(c) p. 2884, Fig. 1; and formulas 2.5–2.7, p. 2871, formulas 3.20–3.22]. The reason is that the distinct term $\Gamma_{11}^{d}(q,t)$ contributes an oscillatory term around $\Gamma_{11}^{s}(q,t)$ in exactly the same way as $S(q,\omega)$ oscillates around $S_s(q,\omega)$ and $S(q)$ around 1 in the q domain that we consider at present $(q/q_0>0.9)$.[6,22] For $\tau_l^s(q)^{-2}$, we have[23]

$$[\tau_l^s(q)]^{-2}=\tfrac{5}{2}q^2v^2+\tau^{-2}, \tag{18}$$

where the q-independent term τ^{-2} is given by

$$\tau^{-2}=\frac{1}{\Omega_0^2}\left\{\frac{n}{3M^2}4\pi\int_0^\infty dr\,r^2g(r)\left[[V''(r)]^2+2\left[\frac{1}{r}V'(r)\right]^2\right]+\frac{1}{6n^2\pi^2}\int_0^\infty dq'(q')^2\{[\gamma_l^d(q')]^2+2[\gamma_t^d(q')]^2\}[S(q')-1]\right\} \tag{19}$$

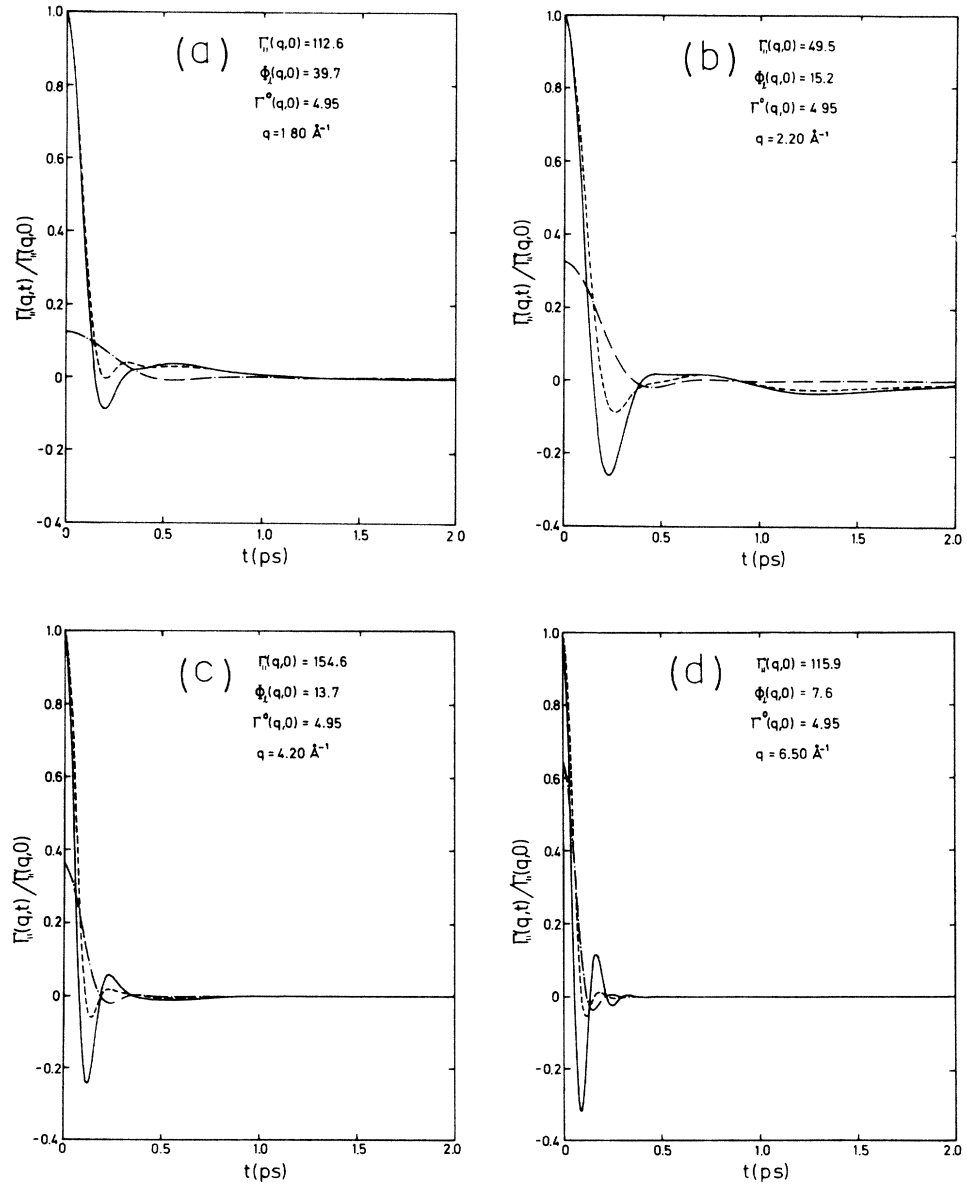

FIG. 11. Memory functions for liquid Pb at 623 K. Results for representative q values are given. $\Gamma_{11}(q,t)$ normalized to $\Gamma_{11}(q,0)$ (solid line); $\Phi_l(q,t)$ normalized to $\Phi_l(q,0)$ (dashed line); $\Gamma^0(q,t)$ normalized to $\Phi_l(q,0)$ (dashed-dotted line). The values of the memory functions at $t=0$ are as given in the figure.

and

$$\gamma_l^d(q') = -\Omega_{q'}^2 , \tag{19'}$$

$$\gamma_t^d(q') = -(n/2M)4\pi \int_0^\infty dr\, r^2 g(r)[V''(r)+(2/r)V'(r)]\sin(q'r)/q'r - \tfrac{1}{2}\gamma_l^d(q) . \tag{19''}$$

We observe that in order to compare theory to experiment, we need information about $V(r)$, $g(r)$, and $S(q)$. These are well enough known for Pb (Ref. 24) at 623 K and Rb (Refs. 25 and 26) at 315 K. We therefore evaluated the necessary functions for these two cases.

In Fig. 11 we give a few representative examples of $\Phi_l(q,t)$, $\Gamma^0(q,t)$, and $\Gamma_{11}(q,t)$ for Pb at 623 K and in Fig. 12 for Rb at 315 K. The timescale is extended only to 2 ps because most of the variation of the various memory functions occur within this time span. It is observed that the initial rapidly decaying part of $\Gamma_{11}(q,t)$ has a half-width at half maximum (HWHM) varying from 0.1—0.2 to 0.03 ps. With increasing q values, $\Gamma_{11}(q,t)$ becomes increasingly narrow and the negative oscillatory feature becomes more pronounced. According to its definition, we expect it to disappear at enough large q values because then

$$q^2\Phi_l(q,t) \rightarrow \Gamma^0(q,t) .$$

$\Gamma_{11}(q,t)$ describes only interactions [compare Eqs.

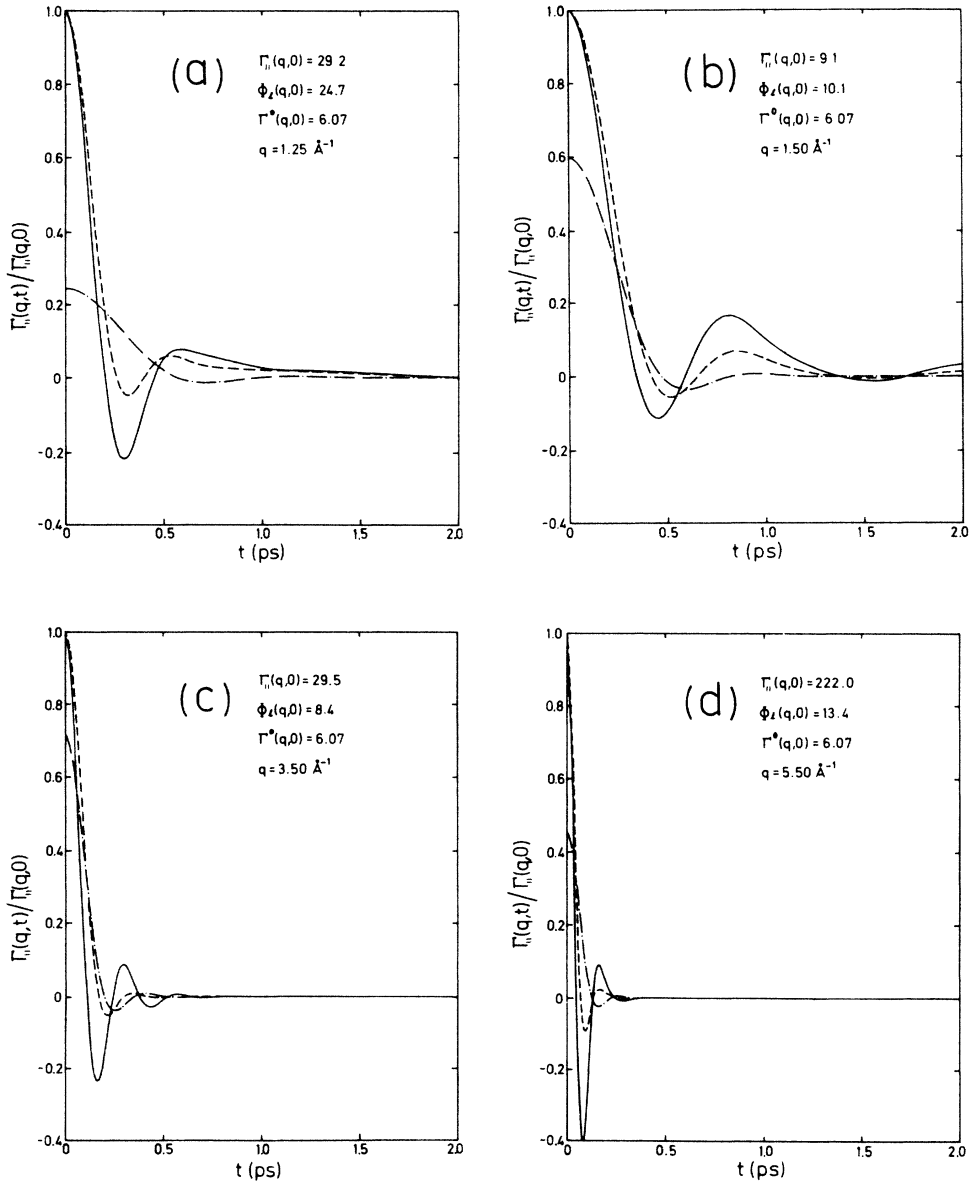

FIG. 12. Memory functions for liquid Rb at 315 K. Results for representative q values are given. Notations are the same as in Fig. 11.

(12)–(14)]. As we see, this transition to free motion will finally occur, but only at a very large q value.

We notice that the approximation for describing the whole $\Gamma_{11}(q,t)$ with a Gaussian form becomes increasingly worse as q increases. On the other hand, the memory function $\Phi_l(q,t)$ is increasingly better approximated with a Gaussian as q increases.

Using Eqs. (18) and (19), $[\tau_l^s(q)]^{-2}$ is evaluated and compared to experimentally determined values of $[\tau_l(q)]^{-2}$. The experimental values of $\tau_l(q)$ follow from the HWHM values of Γ_{11} assuming $\tau_l(q)=W_{\mathrm{HWHM}}/(\ln 2)^{1/2}$. The assumption is then made that the experimentally found functions $\Gamma_{11}(q,t)$ are well described by a Gaussian to a t value corresponding to $W_{\mathrm{HWHM}}/(\ln 2)^{1/2}$. By fitting Gaussians to our memory function Γ_{11}, we have found that this is indeed the case for smaller times. In the theoretical evaluation for Pb at 623 K, the potential with power $n=5$, 12, and 25 is used to calculate $[\tau_l^s(q)]^{-2}$. It should be noticed that the $q=0$ value of $[\tau_l^s(q)]^{-2}$ given as τ^{-2} in Eq. (18) is determined by the various integrals over the potential $V(r)$. The q variation comes from the term $\frac{5}{2}q^2v^2$, which, in turn, contains contributions from free flight, as well as terms from the sixth moment.[23]

In Fig. 13, $[\tau_l^s(q)]^{-2}$ calculated as described is compared to the experimental values of $[\tau_l(q)]^{-2}$. It is seen that the value of τ^2 [Eq. (18)] is sensitively dependent on the shape of the repulsive potential. For $n=25$ the curve falls above the frame of the picture. This is an important conclusion, as no other such *potential sensitive function* was found earlier that can be directly derived from experiment. Thus, for instance, the fourth moment is relatively insensitive, as was demonstrated in Sec. III. It is found that the best value of n in the Jacobs potential is 5, in agreement with the results of the fit to the fourth moment.

It is also found that the theoretical q variation of $[\tau_s(q)]^{-2}$ does not describe the experimental width data well. In order to test if a q^2 variation can at all describe the experimental data, we fitted a curve of form $[\tau_s(q)]^{-2}=aq^2+b$. As seen in Fig. 13, a very good fit is produced for $[\tau_s(q)]^{-2}=12.3q^3+48$. As $a=cv^2$ [Eq. (18)], with $v^2=2.49$ (Å/ps)^2, we find $c=4.95$ instead of $\frac{5}{2}$, as given by the theory; also, $b=48$ instead of 120.

A result of a similar nature is obtained for liquid rubidium, as seen in Fig. 14. The theory does not describe the q variation in the correct way. By fitting the same form as for liquid lead, we find $[\tau_s(q)]^{-2}=15.7q^2+6.2$. As $v^2=3.086$ (Å/ps)^2, one finds that the factor in front of q^2 can be written $5.1v^2$. Thus, in both cases we observe a value of 5 instead of $\frac{5}{2}$ in front of q^2v^2 in Eq. (18).

The fact that the values of $b=\tau^{-2}$ in Eq. (18) come out much smaller than the theoretical values, 2.5–3 times smaller, cannot be taken to be certain, as we do not have experimental points below $q/q_0=0.8$.

Regarding the factor in front of q^2v^2 in Eq. (18), we notice that the first theoretical value [Ref. 5(a), Appendix 1, formula A1.11] was $\frac{1}{2}$, in the next approximation (Ref. 22, p. 404, formula 3.9) it was given as $\frac{5}{2}$, and in this work we find 5. This fact should initiate various comparisons between theory and experiments for larger q value ($q>q_0$).

V. CONCLUSION

We have found that carefully performed neutron scattering studies including accurate correction procedures on several liquid metals allow a detailed analysis

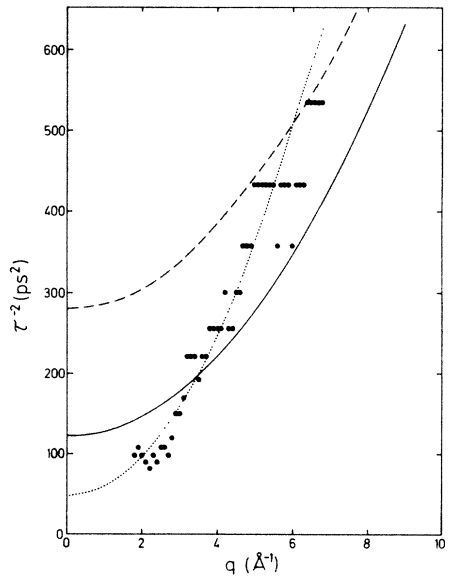

FIG. 13. Results for the width function $\tau_l(q)^{-2}$ from neutron data on liquid Pb at 623 K (●). These data are compared to kinetic-theory data for $\tau_l^s(q)^{-2}$ according to Sjögren's theory for two different forms of $V(r)$ according to Eq. (9) and Table I. $n=12$ (dashed line); $n=5$ (solid line); fitted curve $\tau_s(q)^{-2}=12.3q^2+48$ (dotted line).

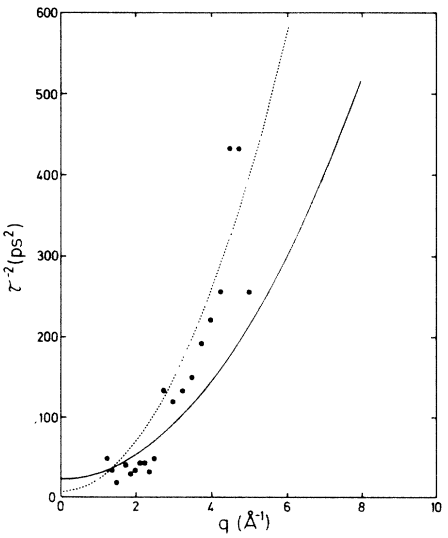

FIG. 14. Results for the width function $\tau_l(q)^{-2}$ from neutron data on Rb at 315 K (●). These data are compared to kinetic-theory data for $\tau_l(q)^{-2}$ according to Sjögren's theory (solid line) and to the fitted curve $\tau_s(q)^{-2}=15.7q^2+6.2$ (dotted line).

involving determination of memory functions for the longitudinal current correlation functions. From these memory functions it is possible to draw conclusions regarding the generalized longitudinal viscosity. Such data combined with MD data can become a powerful aid in the discussion of various model theories such as generalized hydrodynamics and viscoelastic theory. It may also serve as a test on approximations made in advanced kinetic theory in the mode-coupling versions. We have also noticed that the memory functions derived from the more elaborate and detailed kinetic theory is sensitive to the pair-potential form assumed. This seems to be the first case of a noticeably potential-sensitive function derived from neutron scattering functions. We believe that our type of analysis and our results open new possibilities of exploring neutron scattering data in creating a full understanding of fluid mechanics from macroscopic to atomic domains. It is no longer necessary to compare theories to the structureless $S(q,\omega)$, but rather to other more structured, derived quantities.

[1]Narinder K. Ailawadi, A. Rahman, and R. Zwanzig, Phys. Rev. A **4**, 1616 (1971).
[2]W. E. Alley and B. J. Alder, Phys. Rev. A **27**, 3174 (1983).
[3]B. J. Alder, W. E. Alley, and E. L. Pollock, Ber. Bunsenges. Phys. Chem. **85**, 944 (1981).
[4]W. Götze and M. Lücke, Phys. Rev. A **11**, 2173 (1975); W. Götze and A. Zippelius, *ibid.* **14**, 1842 (1976); J. Bosse, W. Götze, and M. Lücke, *ibid.* **17**, 447 (1978); **18**, 1176 (1978).
[5](a) L. Sjögren and A. Sjölander, J. Phys. C **12**, 4369 (1979); (b) L. Sjögren, *ibid.* **13**, 705 (1980); (c) L. Sjögren, Phys. Rev. A **22**, 2866 (1980); **22**, 2883 (1980).
[6]K. E. Larsson, Phys. Chem. Liq. **12**, 273 (1983). This is a review paper with pertinent references.
[7]J. R. D. Copley and J. M. Rowe, Phys. Rev. Lett. **32**, 49 (1974); Phys. Rev. A **9**, 1656 (1974).
[8]O. Söderström, Phys. Rev. A **23**, 785 (1981); O. Söderström, U. Dahlborg, and M. Davidovic, *ibid.* **27**, 470 (1983).
[9]U. Dahlborg and L. G. Olsson, Phys. Rev. A **25**, 2712 (1982).
[10]K. Shibata, S. Hoshino, and H. Fujihita, J. Phys. Soc. Jpn. **53**, 899 (1984).
[11]U. Dahlborg, O. Söderström, W. Gudowski, K. E. Larsson, and M. Davidovic, J. Phys. F **15**, 2053 (1985).
[12]J. R. D. Copley and S. W. Lovesey, Rep. Prog. Phys. **38**, 461 (1975), especially Table A1, p. 556.
[13]O. Söderström, U. Dahlborg, and W. Gudowski, J. Phys. F **15**, L23 (1985).
[14]A. Rahman, Phys. Rev. A **11**, 2191 (1975).
[15]T. E. Faber, *An Introduction to Theory of Liquid Metals* (Cambridge University Press, Cambridge, 1972), p. 167.
[16]J. M. Flinn, Ph.D. dissertation, Catholic University of America, 1969.
[17]U. Balucani, R. Vallauri, T. Gaskell, and M. Gori, Phys. Lett. **102A**, 109 (1984).
[18]M. D. Johnson, P. Hutchinson, and N. H. March, Proc. Phys. Soc. London, Sect. A **202**, 283 (1969).
[19]D. Schiff, Phys. Rev. **186**, 151 (1969).
[20]E. Jacobs and Hans C. Andersen, Chem. Phys. **10**, 73 (1975).
[21]J. P. Boon and S. Yip, *Molecular Hydrodynamics* (McGraw-Hill, New York, 1980).
[22]K. E. Larsson, Phys. Chem. Liq. **9**, 117 (1980), especially pp. 131–133.
[23]G. Wahnström and L. Sjögren, J. Phys. C **15**, 401 (1982); compare Eq. (3.9) and the discussion preceding it.
[24]U. Dahlborg, M. Davidovic, and K. E. Larsson, Phys. Chem. Liq. **6**, 149 (1977).
[25]T. Kinell (private communication). The tabulated Rb potential derived by Price *et al.* (Ref. 24) and used by Rahman in his molecular-dynamic studies were given together with corresponding pair distribution and structure-factor values.
[26]D. L. Price, Phys. Rev. A **4**, 358 (1971); D. L. Price, K. S. Singwi, and M. P. Tosi, Phys. Rev. B **2**, 2983 (1970).